3D tomographic imaging with the γ-eye planar scintigraphic gamma camera

IOP Conf. Series: Journal of Physics: Conf. Series **931** (2017) 012002 doi:10.1088/1742-6596/931/1/012002

3D tomographic imaging with the γ-eye planar scintigraphic gamma camera

H Tunnicliffe[1,2], M Georgiou[3], G K Loudos[4], A Simcox[1,2] and C Tsoumpas[2]

[1]School of Physics and Astronomy, University of Leeds, UK
[2]Division of Biomedical Imaging, School of Medicine, University of Leeds, UK
[3]BET Solutions, Research & Development, Athens, Greece
[4]Department of Biomedical Engineering, Technological Educational Institute of Athens, Greece

Keywords: Single photon emission computed tomography, small animal imaging, QSPECT, STIR.

Abstract: γ-eye is a desktop planar scintigraphic gamma camera (100 mm × 50 mm field of view) designed by BET Solutions as an affordable tool for dynamic, whole body, small-animal imaging. This investigation tests the viability of using γ-eye for the collection of tomographic data for 3D SPECT reconstruction. Two software packages, QSPECT and STIR (software for tomographic image reconstruction), have been compared. Reconstructions have been performed using QSPECT's implementation of the OSEM algorithm and STIR's OSMAPOSL (Ordered Subset Maximum A Posteriori One Step Late) and OSSPS (Ordered Subsets Separable Paraboloidal Surrogate) algorithms. Reconstructed images of phantom and mouse data have been assessed in terms of spatial resolution, sensitivity to varying activity levels and uniformity. The effect of varying the number of iterations, the voxel size (1.25 mm default voxel size reduced to 0.625 mm and 0.3125 mm), the point spread function correction and the weight of prior terms were explored. While QSPECT demonstrated faster reconstructions, STIR outperformed it in terms of resolution (as low as 1 mm versus 3 mm), particularly when smaller voxel sizes were used, and in terms of uniformity, particularly when prior terms were used. Little difference in terms of sensitivity was seen throughout.

1. Introduction

The γ-eye camera is a compact desktop gamma camera designed by BET Solutions as an affordable tool for research teams carrying out preclinical trials on small rodents. While planar imaging is arguably sufficient for many trials [1], with the addition of a rotating bed the system could be used to collect tomographic data by rotating the subject rather than the camera as in most SPECT (single photon emission computed tomography) systems. The advantages of this being that the tomographic images have a higher contrast than planar images [2,3] and as a 3D image is constructed, the subject can be analysed from multiple views.

Various analytic or iterative methods can reconstruct projections acquired at different angles of view into a 3D image. While analytic methods such as filtered back projection (FBP) are much faster, iterative methods offer several advantages, including the ability to model the emission and detection process, allowing for superior image quality and the absence of streak artefacts that are inherent with FBP. The most widely used iterative algorithm is the ordered

[2]To whom any correspondence should be addressed: c.tsoumpas@leeds.ac.uk

subset expectation method (OSEM) [4]. Additionally, there are maximum a posteriori (MAP) algorithms which use a prior term to suppress noise of the reconstructed image [5].

The suitability of γ-eye for use as a SPECT system has been assessed by converting projection data from γ-eye to sinogram data suitable for reconstruction and then, converting the sinograms into a format compatible with tomographic reconstruction software [6]. By performing reconstructions and analysing the resulting images, attempts could be made to optimize the images in terms of resolution, contrast, noise reduction and reconstruction time.

2. Methods

2.1 The γ-eye camera

γ-eye has 100×50 mm^2 field of view and a hexagonal, parallel hole collimator (26 *mm* depth & 1.5 *mm* hole diameter). The detector consists of a CsI(Na) pixelated scintillator coupled to two position-sensitive photomultiplier tubes [1].

2.2 Reconstruction software

Two different software packages for SPECT image reconstruction were investigated, QSPECT [7] and STIR[8,9]. QSPECT is an open-source package that offers a simple user interface for iterative SPECT reconstruction via an implementation of OSEM. STIR contains two algorithms for iterative image reconstruction, OSMAPOSL (Ordered Subset Maximum A Posteriori One Step Late) and OSSPS (Ordered Subset Separable Paraboloidal Surrogate). The OSMAPOSL algorithm is a refined OSEM style algorithm that can optionally include prior terms [10]. Where the use of prior terms has been explored, the quadratic Gibbs prior was used with value p controlling the weight of the prior term. OSSPS implementation [11] uses the formula:

$$\lambda^{new} = \lambda + \zeta D \nabla \Psi \tag{1}$$

where λ is the parameters to be estimated, Ψ is the objective function, D is the diagonal matrix and ζ is the iteration dependant relaxation parameter given by the relaxation parameter α and the relaxation gamma γ in the formula

$$\zeta = \frac{\alpha}{1 + \gamma n} \tag{2}$$

2.3 Data sets and analysis

Three sets of data were used to assess the performance of the reconstruction software. A single capillary tube; a phantom with three cylindrical regions, each with different activity levels and finally a mouse. Each dataset consisted of 36 projections, taken at rotational increments of 10° from the last and a rotational distance of 5 *cm* and used ^{99m}Tc solution. The capillary tube was filled with 150 μCi of radiation. The capillary dataset was used to measure the spatial resolution achieved by various reconstructions. To do this a Gaussian fit was applied to the line profile of each reconstructed image from which the full-width-half-maximum (FWHM) could be extracted. While there are other methods that can provide optimised fitting for the point spread function [12], Gaussian fitting is sufficient for comparison purposes. The mean FWHM of numerous line profiles along the length of the capillary were used to give a value for the spatial resolution of each reconstruction [13]. The next data set was a phantom, with three shallow cylindrical wells. Each was filled with a different level of activity to give three regions of varying intensity (bright: 500 μCi, middle: 250 μCi and dim: 125 μCi). This was used to assess the uniformity achieved and the sensitivity to varying levels of activity of different reconstructions. Uniformity was assessed by measuring the coefficient of variation (COV = σ/μ) within each region and the sensitivity through comparison of the mean number in each region.

3. Results and Discussion

3.1 Spatial resolution

The spatial resolution achieved by various reconstructions across a number of iterations is shown in Figure 1a. In all cases, the resolution improves with the number of iterations, with the improvement in resolution stabilized at high iteration numbers. STIR reconstructions use the OSMAPOSL algorithm with no prior term (equivalent to OSEM). STIR provides reconstructed images with higher resolution in comparison to QSPECT, because STIR includes point spread function (PSF) [14,15]. The QSPECT reconstructions make use of a ray-tracing methodology which is

described by Loudos [16] achieving resolution of 3 *mm*, whereas resolutions as low as 1 *mm* were observed with STIR. QSPECT however, outperformed STIR in terms of speed with the fastest STIR (61.48 *s*) reconstruction taking 6 times longer than QSPECT (9.68 *s*) over 15 iterations. FBP images had a resolution of 4 *mm*. STIR PSF correction is dependent on the collimator, the slope and σ_0, as illustrated by the equation:

$$\sigma(d) = slope \times d + \sigma_0 \quad (3)$$

where $\sigma(d)$ is the sigma (related to the width) of the Gaussian blur at height d above the collimator. The PSF values were calculated as part of an investigation into planar imaging with the γ-eye camera. The σ in a planar image of a capillary was measured at different heights above the collimator and a linear fit gave values for the slope and σ_0.

The choice of 2D (slices corrected sequentially) or 3D (correction between slices) PSF was also investigated. No significant difference was seen in the resolution in the x-y plane between the 2D and 3D PSF options, differences may be seen if the z-axis resolution was investigated. While no significant difference in resolution was measured between 2D and 3D correction, the 3D PSF lead to a 13 times increase in reconstruction time over 15 iterations.

STIR allows the voxels of reconstructed images to have dimensions different to the original projections. The transverse voxel dimensions were reduced from 1.25 *mm* to 0.625 *mm* and 0.3125 *mm*. The axial dimension remained at 1.25 *mm* throughout. The 0.625 *mm* voxel size demonstrated significant improvements in resolution over the 1.25 *mm* voxel size but at the cost of 4 times increase in reconstruction time (from 61.48 *s* to 250.86 *s* for 15 iterations). The 0.3125 *mm* voxels gave a marginal improvement in resolution over the 0.625 *mm* but at the cost of a 19 times increase in reconstruction time compared to 1.25 *mm* voxels (from 61.48 *s* to 1175.41 *s* for 15 iterations). (Note, all reconstructions ran on Intel® Core™ i7-3632QM CPU 2.20GHz with 8.00 GB RAM).

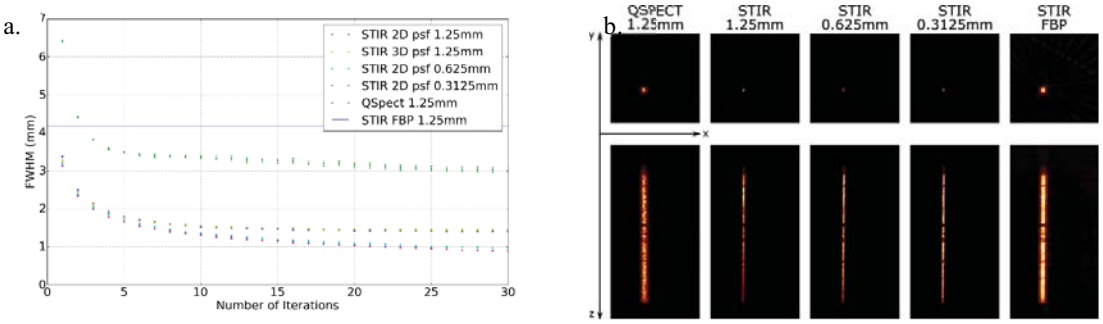

Figure 1a. Mean FWHM of Gaussian fit against number of iterations for different reconstruction settings (QSPECT OSEM and STIR OSMAPOSL). **b.** Comparison of reconstructed capillary images with different software and settings after 15 iterations.

3.2 Sensitivity and Uniformity

The QSPECT reconstruction of the 3 well phantom resulted in a more uniform image than the most comparable STIR reconstruction (STIR OSEM 1.25 *mm*), as demonstrated by the smaller COV values for all three regions. The ratios between the mean values for the different regions are relatively consistent between QSPECT and STIR suggesting that there is little difference in the sensitivity to varying levels of radiation between the two.

Table 1. Mean and COV values for each phantom region for different reconstruction settings.

	Bright region		**Middle Region**		**Dim Region**	
Reconstruction (20 iterations)	**Mean**	**COV**	**Mean**	**COV**	**Mean**	**COV**
QSPECT OSEM	9.26	0.22	3.78	0.38	2.43	0.38
STIR OSEM 1.25 *mm*	9.26	0.26	3.72	0.54	2.53	0.46
STIR OSEM 0.625 *mm*	9.29	0.26	3.73	0.54	2.54	0.46
STIR OSMAPOSL-QP 0.625 *mm* (p=0.5)	9.12	0.16	3.73	0.34	2.51	0.33
STIR OSMAPOSL-QP 0.625 *mm* (p=0.75)	9.09	0.16	3.73	0.31	2.50	0.30
STIR OSMAPOSL-QP 0.625 *mm* (p=1)	9.06	0.16	3.73	0.29	2.50	0.29

The effect of varying the voxel size on sensitivity and uniformity has also been explored. Table 1 shows minimal changes in the COV between the 1.25 mm and 0.625 mm reconstructions suggesting that changes in voxel size have little effect on the uniformity of the resulting image. The mean values also remain very similar, indicating that the sensitivity is also largely unaffected. It should be noted that the mean values for the smaller voxel sizes have been scaled to adjust for the difference in the total number of voxels in the active area.

To improve the uniformity of the images, the use of prior terms has been explored. Here the quadratic prior term from the STIR toolkit has been used, the weight of the prior term can be adjusted by changing the value of the penalization factor (*p*). As can be seen in Figure 2, the use of prior terms has a strong effect on the uniformity. This is supported by the reduction in the COV values for all regions. As expected the higher the penalization factor, lower COV values are measured and the images are more uniform, although the change in the COV is not significant in the bright region between the different penalisation factors used. With the use of prior terms, more uniform images can be achieved with STIR than were achieved with QSPECT.

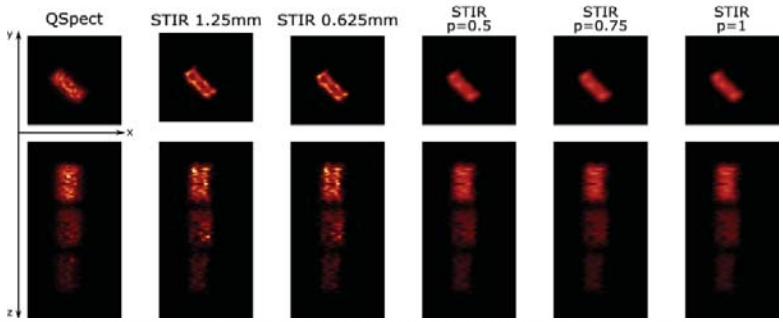

Figure 2. Reconstructed images of the 3 well phantom with varying activity levels for different settings. STIR reconstruction use OSMAPOSL with no prior term. (20 iterations)

3.3 Mouse Data

Figure 3 shows the same slice from various reconstructions of the mouse lung data set. Some issues were found with this data set resulting in circular defects that could not be fully removed by the centre of rotation correction. This is believed to be due to alignment issues from the capture of the projections. For this reason, a single slice with minimal defects was selected for analysis. All STIR reconstructions used 0.625 *mm* voxel size and 2D PSF correction for best performance. Reconstructions were performed for up to 20 iterations (except OSSPS).

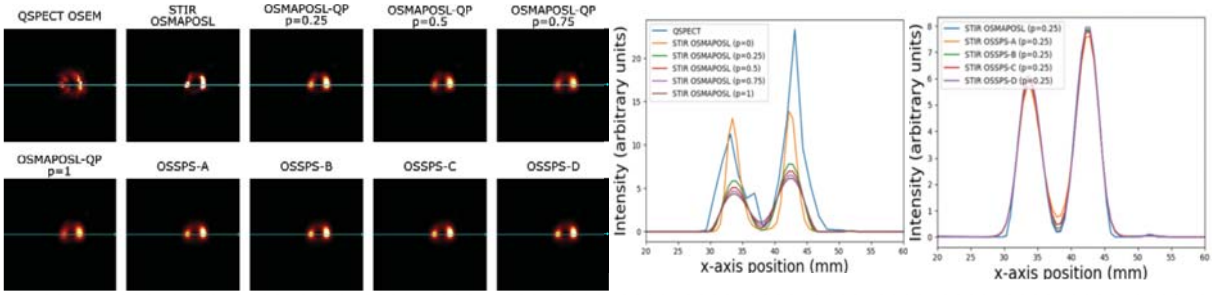

Figure 3. Reconstructed image slice from the mouse lung data set for different reconstruction settings. Blue line represents line profile shown in the right-hand side profiles.

STIR produced clearer images than QSPECT with increased resolution allowing for less grainy images and better separation between the two lungs. A variety of prior penalisation factors were tested, ranging from 0.25 to 1. The use of prior terms produced less distorted images., however, higher penalization factors have a blurring effect on the images. This is evident in Figure 3 a where the higher *p* values have less separation between the two lungs.

For OSSPS, an initial image, created by 2 iterations of OSMAPOSL algorithm was used to aid convergence, followed by 10 iterations of OSSPS. Quadratic prior terms were used with a penalization factor of 0.25. The first reconstruction (OSSPS-A) used the default relaxation parameters provided by STIR. Each subsequent reconstruction used slightly altered values, to improve the resulting image. The OSSPS images in Figure 3 are similar to those produced by OSMAPOSL when using the prior term. However, the noise may not have been suppressed sufficiently, as there is a slightly brighter region between the lower part of the lungs. Line profiles from the OSSPS images are shown in Figure 3. In these the reconstruction seems near identical to the OSMAPOSL with $p = 0.25$ which may suggest that much of the final image was determined by the initial image used.

The parameters used in OSSPS-A ($\alpha = 1$, $\gamma = 0.1$) gave a marginally worse reconstruction than OSMAPOSL, the bright regions being slightly less bright and the centre region being slightly brighter (Figure 3). First, the α was increased for OSSPS-B ($\alpha = 2$, $\gamma = 0.1$), giving an increase in brightness for the lungs and a decrease in brightness for the region between. Following this γ was increased (OSSPS-C: $\alpha = 2$, $\gamma = 0.2$), this gave slightly worse results in terms of these two factors. Instead a lower value of γ was tried (OSSPS-D: $\alpha = 2$, $\gamma = 0.05$), this gave the best reconstruction overall, but the differences are again very slight.

4. CONCLUSIONS

Successful reconstructions of phantom SPECT data acquired with the γ-eye using both STIR and QSPECT software packages have been demonstrated. Initial issues with the misalignment of the centre of rotation were successfully corrected for through adjustment of sinogram data. However, this failed to correct for all defects in the mouse data, proper geometrical calibration should correct this.

The comparisons of images produced by both packages demonstrate that, for most cases, STIR would be the better choice. Better results in terms of resolution (STIR: 1 *mm*, QSPECT: 3 *mm*) and uniformity (when prior terms are used), were achieved with STIR. However, very little difference was found in the sensitivity to different activity levels and the QSPECT reconstructions were 26 times faster than STIR for the resolutions stated. The mouse lung images demonstrate that the image resolution achievable with the γ-eye camera is sufficient for use with small animal imaging where individual organs must be resolved. Interesting results were seen from OSSPS in that is matched the quality of the OSMAPOSL results in fewer iterations.

5. REFERENCES

[1] Georgiou M, Fysikopoulos E, Mikropoulos K, Fragogeorgi E and Loudos G 2016 *Mol. Imaging Biol.*
[2] Dowsett D J, Kenny P A and Johnston R E 2006 *Hodder Arnold* 469–510
[3] Lavely W C, Goetze S, Friedman K P, Leal J P, Zhang Z, Garret-Mayer E, *et al* 2007 *J. Nucl. Med.* **48** 1084–9
[4] Hudson H M and Larkin R S 1994 *IEEE Trans. Med. Imaging* **13** 601–9
[5] Bruyant P P 2002 *J. Nucl. Med.* **43** 1343–58
[6] Todd-Pokropek A, Cradduck T D and Deconinck F 1992 *Nucl. Med. Commun.* **13** 673–99
[7] Loudos G K, Papadimitroulas P, Zotos P, Tsougos I and Georgoulias P 2010 *Nucl. Med. Commun.* **31** 558–66
[8] Thielemans K, Tsoumpas C, Mustafovic S, Beisel T, *et al* 2012 *IEEE Nucl. Sci. Symp. Conf. Rec.* **4** 2174–6
[9] Fuster B M, Falcon C, Tsoumpas C, Livieratos L, Aguiar P, Cot A, *et al* 2013 *Med. Phys.* **40** 92502
[10] Jacobson M, Levkovitz R, Ben-Tal A, Thielemans K, Spinks T, *et al* 2000 *Phys. Med. Biol.* **45** 2417-39
[11] Mustafovic S and Thielemans K 2004 *IEEE Trans. Med. Imaging* **23** 433–46
[12] Fountos, G P, Michail C M, Zanglis A, Samartzis A, Martini N, *et al* 2012 *Med. Phys.* **39** 1561-70
[13] Dinelle K, Thielemans K, Tsoumpas C and Spinks TJ 2004 *IEEE Nucl. Sci. Symp. Conf.* **44** 4043–7
[14] Pareto D, Cot A, Falcón C, Juvells I, Pavía J and Ros D 2002 *IEEE Trans. Nucl. Sci.* **49** 17–24
[15] Pareto D, Cot A, Pavía J, Falcón C, Juvells I, *et al* 2003 *Eur. J. Nucl. Med. Mol. Imaging* **30** 1322–9
[16] Loudos G K 2008 *Comput. Med. Imaging Graph.* **32** 83–94